PCCP

Accepted Manuscript




ROYAL SOCIETY OF CHEMISTRY

www.rsc.org/pccp

Journal Name

ARTICLE

# Two Phosphonium Ionic Liquids with High $Li^+$ Transport Number

Vitor L. Martins*, Nédher Sanchez-Ramirez, Mauro C. C. Ribeiro and Roberto M. Torresi**

Received 00th January 20xx,
Accepted 00th January 20xx

DOI: 10.1039/x0xx00000x

www.rsc.org/

This work presents the physicochemical characterization of two ionic liquids (ILs) with small phosphonium cations, triethylpenthylphosphonium bis(trifluoromethanesulfonyl)imide ($[P_{2225}][Tf_2N]$) and the (2-methoxyethyl) trimethylphosphonium bis(trifluoromethanesulfonyl)imide ($[P_{222(2O1)}][Tf_2N]$), and their mixtures with $Li^+$. Properties such as the electrochemical window, density, viscosity and ionic conductivity are presented. The diffusion coefficient was obtained by two different techniques, PGSE-NMR and Li electrodeposition with microelectrodes. In addition, the $Li^+$ transport number was calculated by the PGSE-NMR technique and by an electrochemical approach. The use of these three techniques showed that the PGSE-NMR technique underestimates the diffusion coefficient for charged species. The $Li^+$ transport number found to be as high as 0.54. Raman spectroscopy and molecular dynamics simulations were used to evaluate the short-range structure of the liquids. These experiments suggested that the interaction between $Li^+$ and the $Tf_2N^-$ anion is similar to that with other ILs containing the same anion. However, the MD simulations also showed that the $Li^+$ ions interact differently with the cation containing an alkyl ether chain. The results found in this work suggest that these $Li^+$ mixtures have promising potential to be applied as electrolytes in batteries.

## Introduction

Ionic liquids (ILs) are salts that possess melting points below 100 °C and are compounds that contain only ions. This means that they possess intrinsic ionic conductivity, which makes them an interesting alternative to be used as electrolytes. In addition, they have high chemical and thermal stability and extremely low vapour pressure.[1–3] Among the cations that form ILs, imidazolium is one of the most common and investigated cations by research groups in different areas, especially energy storage devices.[4–9] The anion bis(trifluoromethanesulfonyl) imide ($Tf_2N^-$) has also been broadly investigated since the ILs formed by this anion possess low viscosity and high ionic conductivity; moreover, they are hydrophobic.[10–12]

With the aim to apply these ILs as Li-ion battery electrolytes, one must consider the mixture of these liquids with $Li^+$ salt and understand the effect of this addition to the physicochemical properties of the mixture. Many research groups have investigated this effect in ILs containing imidazolium and $Tf_2N^-$. They reported an undesirable effect in the transport properties when $Li^+$ salt is added to the IL. Specifically, the viscosity increases as $Li^+$ is added, which results in a decrease of the ionic conductivity relative to the neat ILs.[13–15] Because of the high viscosity and low ionic conductivity at room temperature for ILs comprised of imidazolium and $Tf_2N^-$ make this IL unsuitable for application as Li-ion battery electrolytes, the search for other ILs remains open.

Normally, large phosphonium cations with high viscosity are reported in the literature,[16–20] but some small phosphonium cations have also been reported.[21–24] ILs containing small phosphonium cations possess lower viscosity and thus demonstrate promise for application as electrolytes. Tsunashima and Sugiya[21] presented a comparative study involving some small phosphonium ILs and ammonium ILs. Both ILs contained the $Tf_2N^-$ anion. They found that the phosphonium ILs have lower viscosities and higher ionic conductivities than the ammonium analogues. Later, Seki *et al.*[22] found similar results. Girard *et al.*[23] showed the physicochemical properties of a small phosphonium cation ($P_{111i4}^+$) containing a different anion (bis(fluorosulfonyl)imide) with different amounts of $Li^+$ salt. They found a high electrochemical stability for the neat IL at room temperature and high lithium deposition-dissolution efficiency at 100 °C.

In this work, we show the physicochemical properties of two ILs containing phosphonium cations: one with an alkyl side chain, triethylpenthylphosphonium ($P_{2225}^+$), and other with an alkyl ether side chain, (2-methoxyethyl)trimethylphosphonium ($P_{222(2O1)}^+$). Both ILs contain the anion $Tf_2N^-$. Figure 1 depicts the ions investigated in this study. In addition, $Li^+$ mixtures (1.0 and 2.0 mol $L^{-1}$) were prepared and analyzed with same techniques. The $Li^+$ transport number was evaluated with different approaches, and the results suggest that these mixtures show promise as Li-ion battery electrolytes.

*Instituto de Química, Universidade de São Paulo - C.P. 26077, CEP 05513-970, São Paulo, SP, Brazil.*
**martinsv@iq.usp.br; **rtorresi@iq.usp.br*
Electronic Supplementary Information (ESI) available. In addition, all data presented in this work are available in supplementary tables.
See DOI: 10.1039/x0xx00000x

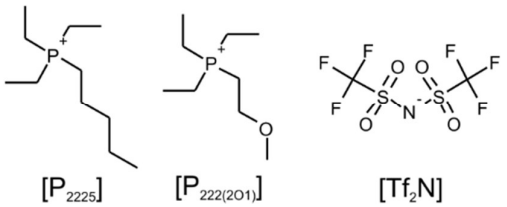


Figure 1. Ions of the ionic liquids $[P_{2225}][Tf_2N]$ and $[P_{222(2O1)}][Tf_2N]$ used in this work.

## Materials and Methods

### Synthesis of $[P_{222x}][Tf_2N]$

The phosphonium ILs were synthesized as described elsewhere.[21] Briefly, 85 mmol of triethylphosphina (20% v/v in toluene, Sigma-Aldrich) were reacted with 85 mmol of 1-bromopentane (99%, Sigma-Aldrich) or 2-bromo-ethylmethylether (99%, Sigma-Aldrich) in an Ar atmosphere for five hours under mechanical agitation at 80 °C. Subsequently, 20 mL of hexane was added to the reaction mixture and the resulting crystals were filtered and dried at 25 °C for 24 hours. Then, 26 mmol of $P_{222x}Br$ were dissolved in 50 mL of water and mixed with 26 mmol of $LiTf_2N$ (99.9%, Sigma-Aldrich) dissolved in 50 mL of water. The mixture was stirred for two hours. The resultant IL is immiscible in water and was separated with dichloromethane. The phase containing the IL was washed five times with water, stirred with activated carbon for two hours and subjected to a chromatography column. The ILs were dried under vacuum at 70 °C for several days until the amount of water was under 100 ppm, which was quantified by the Karl-Fischer coulometric titration (Metrohm).

$Li^+$ mixtures were prepared dissolving the appropriate amount of $LiTf_2N$ in the IL to obtain a mixture of 1.0 and 2.0 mol $L^{-1}$. The mixtures were dried as the neat ILs.

All chemicals were used as received. Solvents were obtained from Synth (Brazil). Only purified water (18 MΩ cm) was used.

The neat ILs will be referred to as $[P_{222x}][Tf_2N]$ to facilitate identification of the ions. The $Li^+$ mixtures will be referred to as molar fraction formulas. For example, the 1.0 mol $L^{-1}$ mixture is $[Li]_{0.25}[P_{222X}]_{0.75}[Tf_2N]$ and the 2.0 mol $L^{-1}$ mixture is $[Li]_{0.39}[P_{222X}]_{0.61}[Tf_2N]$.

**$P_{2225}Br$** data. Exp.: C, 48.7; H, 9.85. Calc for $C_{11}H_{26}BrP$: C, 49.1; H, 9.73; ν (ATR) / $cm^{-1}$: 2962; 2914; 2882; 2814; 1456; 1415; 1390; 1283; 1257; 1108; 1085; 1052; 1020; 810; 776; 734; 616; $\delta_H$ (300 MHz; $D_2O$; ppm): 0.88–0.93 (3H; t; *J*=7.5 Hz); 1.18–1.29 (9H. m); 1.33–1.67 (6H. m); 2.14–2.28 (8H; m); $\delta^{13}_C$ (300 MHz; $D_2O$; ppm): 7.50 (3C); 14.1–13.5 (3C; d; $^1J_{CP}$ = 50 Hz ); 15.9; 19.8–19.1 (1C; d; $^1J_{CP}$ = 47 Hz); 23.1; 24.1; 35.0. NMR spectra presented in Figures S1a and b.

**$[P_{2225}][Tf_2N]$** data. Exp.: C, 33.2; H, 5.63; N, 3.08. Calc for: $C_{13}H_{26}F_6NO_4PS_2$: C, 33.3; H, 5.58; N, 2.98; ν (ATR)/$cm^{-1}$: 3644; 3562; 2961; 2939; 2877; 1467; 1414; 1352; 1332; 1226; 1195; 1139; 1108; 1058; 807; 786; 740; 654; 618; 603; 571; 514; 409; $\delta_H$ (300 MHz; $CD_3CN$; ppm): 0.89–0.94 (3H; t; *J* = 7.5 Hz); 1.12–1.23 (9H; m); 1.33–1.56 (6H; m); 2.01–2.17 (8H; m); $\delta^{13}_C$ (300 MHz; $CD_3CN$; ppm): 5.77 (3C); 12.5–11.8 (3C; d; $^1J_{CP}$ = 48 Hz); 14.1; 17.6–18.3 (1C; d; $^1J_{CP}$ = 47 Hz); 21.5; 22.6; 33.5; 127.4–114.7 (1C; q; $^1J_{CF}$ = 318). NMR spectra presented in Figures S2a and b.

**$P_{222(201)}Br$** data. Exp.: C, 41.3; H, 8.73. Calc for $C_9H_{22}BrOP$: C, 42.0; H, 8.62; ν (ATR) / $cm^{-1}$: 2994; 2975; 2935; 2907; 2882; 2817; 2801; 2756; 1460; 1448; 1432; 1414; 1390; 1292; 1255; 1233; 1179; 1146; 1100; 1047; 1006; 979; 951; 815; 798; 784; 767; 733; 707; 616; 434; $\delta_H$ (300 MHz; $D_2O$; ppm): 1.22–1.33 (9H; m); 2.25–2.37 (6H; m); 2.54–2.67 (2H; m); 3.43 (3H; s); 3.80–3.90 (2H; m) ; $\delta^{13}$c (300 MHz; $D_2O$; ppm): 4.96 (3C; s); 11.6–12.2 (3C; d; $^1J_{CP}$ = 49 Hz); 18.2–18.9 (1C; d; $^1J_{CP}$ = 49 Hz); 58.46; 65.02. NMR spectra presented in Figures S3a and b.

**$[P_{222(201)}][Tf_2N]$** data. Exp.: C, 28.8; H, 4.82; N, 3.04. Calc for $C_{11}H_{22}F_6NO_5PS_2$: C, 28.9; H, 4.85; N, 3.06; ν (ATR) / $cm^{-1}$: 3636; 3563; 2987; 2954; 2930; 2892; 2839; 2821; 1489; 1461; 1415; 1386; 1353; 1332; 1227; 1196; 1139; 1117; 1058; 949; 786; 740; 655; 618; 603; 571; 514; $\delta_H$ (300 MHz; $CD_3CN$; ppm): 1.13–1.25 (9H; m); 2.10–2.22 (6H; m); 2.36–2.44 (2H; m); 3.33 (3H; s); 3.63–3.73 (2H; m); $\delta^{13}_C$ (300 MHz; $CD_3CN$; ppm): 5.84 (3C; s); 12.7–13.4 (3C; d; $^1J_{CP}$ =49 Hz); 19.5–20.2 (1C; d; $^1J_{CP}$ = 49 Hz ); 59.2; 65.8; 127.4–114.7 (2C; q; $^1J_{CF}$ = 319 Hz). NMR spectra presented in Figures S4a and b.

### Measurements

*Electrochemical stability* was determined by linear voltammetry of glassy carbon at 10 mV $s^{-1}$ starting from an open circuit potential until the density current reached ± 150 μA $cm^{-2}$. The stability was determined by a linear sweep starting at the OCP and moving to the positive or negative potentials. Platinum and silver were used as the counter and reference electrodes, respectively. Experiments were performed inside a glovebox filled with Ar ($O_2$ and $H_2O$ < 0.1 ppm) with an Autolab PGSTAT 30 (Metrohm).

*Density and viscosity* were measured with a Viscosimeter SVM 3000 (Anton Paar). *Ionic conductivity* was determined by electrochemical impedance spectroscopy (EIS) of two parallel Pt electrodes with an Autolab PGSTAT 30 in the frequency range of 0.1–100000 Hz. The cell constant was determined with a standard KCl solution.

*Diffusion coefficients* were determined by pulsed gradient spin-echo nuclear magnetic resonance (PGSE-NMR) in a Varian INOVA 300 spectrometer equipped with a 5 mm indirect detection probe (22 G $cm^{-1}$ max) and calibrated with water (2.299 $10^{-9}$ $m^2$ $s^{-1}$) at 298 K. A stimulated spin-echo pulse sequence, 90°-$\tau_1$-90°-$\tau_2$-90°-$\tau_1$ acquisition was used, incorporating a gradient pulse in each $\tau_1$ period. The diffusion coefficient of $Li^+$ was also determined by electrodeposition of Li in Pt microelectrodes, which were fabricated from Pt fibers with different diameters (99%, Roberplat, Brazil) according to procedure described elsewhere.[25]

The *transport number* of $Li^+$ was also calculated by electrochemical impedance spectroscopy (EIS) and dc polarization, as developed by Evans, Vincent and Bruce.[26] This technique is addressed in the Results and Discussions section, and additional details can be find elsewhere.[27]

*Raman spectra* were obtained with a Jobin-Yvon T64000 Raman spectrometer excited with the 647.1 nm line of a $Kr^+$

ion laser with an output power of 400 mW and a resolution of 0.62 $cm^{-1}$.

#### Computational Details

The Molecular Dynamics (MD) simulations were performed with the DL_POLY software package.[28] The potential energy function takes into account the intermolecular Lennard-Jones and Coulombic interactions, as well as the intramolecular properties of bond stretching *r*, angle bending $\theta$, and torsion of the dihedral angles $\psi$,

$$V_{total} = \sum_{i,j;i<j}\left\{4\epsilon_{ij}\left[\left(\frac{\sigma}{r_{ij}}\right)^{12}-\left(\frac{\sigma}{r_{ij}}\right)^{6}\right]+\frac{q_i q_j}{r_{ij}}\right\}+\sum_{bonds}\frac{k_b}{2}(r-r_{eq})^2+\sum_{angles}\frac{k_\theta}{2}(\theta-\theta_{eq})^2+\sum_{dihedrals}k_\psi[1+cos(n\psi-\delta)] \quad (1)$$

where $r_{ij}$ is the distance between atoms *i* and *j* of different ions. Parameters such as the bond lengths $r_{eq}$, angles $\theta_{eq}$, dihedral angles $\psi_{eq}$, and force constant parameters are based on the model of Liu *et al.*[29] for the phosphonium cations, the model of Lopes and Pádua[30] for the $Tf_2N^-$ anion and the model of Aaqvist[31] for the $Li^+$ cation.

The simulations were conducted in cubic boxes generated by Packmol[32] with a random configuration at 298 K with 400 ions in total. Neat ILs were simulated with 200 pairs, and $Li^+$ mixtures were simulated with the replacement of 51 cations with $Li^+$. Pre-equilibrated steps were performed at 350 K to improve the randomness of the system. Then, the temperature was set to 298 K and equilibrated in an NPT ensemble using Berendsen's thermostat and barostat to reach an average pressure of 0.1 MPa and the expected density for this temperature. An additional 1 ns simulation was performed in an NVE ensemble prior to the 6 ns of the production runs. All equilibration and production routines were performed with a time step of 1.0 fs with an equation of motion integrated with the Verlet algorithm.[33]

The equilibrated systems in NPT ensembles attained densities similar to those found experimentally, demonstrating that the MD simulations yield reliable results with respect to the local structure in the liquids.

The partial radial distribution functions (rdf), combined distribution functions (cdf), and spatial distribution functions (sdf) were calculated by the Travis software package.[34]

## Results and Discussion

#### Electrochemical Stability and Density

The electrochemical stability of the ILs was determined by linear voltammetry, the result of which can be seen in Figure S5. Both ILs have wide electrochemical windows, wherein $[P_{2225}][Tf_2N]$ registers 4.9 V and $[P_{222(2O1)}][Tf_2N]$ registers 4.1 V of the electrochemical window. It is a wider electrochemical window than some ILs containing imidazolium [12] and is closer to other ILs containing ammonium cations.[35] The side chain that contains ether causes a diminution of the electrochemical window, as previously reported by Monteiro *et al.*[36]

Figure 2a and b present the densities of $[P_{2225}][Tf_2N]$, $[P_{222(2O1)}][Tf_2N]$ and their $Li^+$ mixtures in a range of temperatures. The density has a linear dependence with temperature for all of the studied systems; specifically, the density decreases as the temperature increases. The addition of $Li^+$ causes an increase in the density in equal proportions at all temperatures. When 1.0 mol $L^{-1}$ of $LiTf_2N$ is added to $[P_{2225}][Tf_2N]$ and $[P_{222(2O1)}][Tf_2N]$, the density increases by 5.7% and 5.0%, respectively. When 2.0 mol $L^{-1}$ of $LiTf_2N$ were added to $[P_{2225}][Tf_2N]$ and $[P_{222(2O1)}][Tf_2N]$, the density increases by 11% and 8.8 %, respectively (see Figure S6).

Ye and Shreeve[37] proposed the following equation to predict the density of a variety of ILs:

$$\rho_{calc.} = \frac{W}{0.6022\,V} \quad (2)$$

where $\rho_{calc.}$ is the calculated density, *W* is the molar mass and *V* is sum of the proposed volume of each species present in the liquid. Using the volumes proposed by Ye and Shreeve for each constituent of the ILs, we can assume that the volume of $[P_{2225}]$ is 359 $Å^3$, $[P_{222(2O1)}]$ is 313 $Å^3$, $[N_{2225}]$ is 332 $Å^3$, $[N_{222(2O1)}]$ is 286 $Å^3$, $[Tf_2N]$ is 248 $Å^3$ and $Li^+$ is 1.99 $Å^3$.[37]

Table 1 summarizes the experimental density at 298 K and the calculated density for all ILs and $Li^+$ mixtures studied in this work. Data for the ammonium analogues is also reported, only for comparison.[22,35]

Because the ILs containing phosphonium possess a heavier and more voluminous cation than the ILs that contain ammonium, the first type of IL must be less dense, which is what we observe. When the $Li^+$ cation replaces one of the phosphonium cations in the system, one must consider the large difference of volume between each species. This difference leads to an increase in the density of the system. In addition, the close interaction between $Li^+$ and the anion $Tf_2N^-$ decreases the volume of the system. The calculated density is lower by 1.7%, on average, than the experimental density for all of the systems investigated. This suggests that equation (2) underestimates the densities values for these systems.

Equation (2) proposed by Ye and Shreeve[37] provides a value relatively close to the experimental value only considering the theoretical volume of each ion. However, because the equation does not consider the interactions among the ions, the calculated density will be smaller than the experimental value, since these interactions will result in a lower volume and higher density than would otherwise be predicted.

#### Viscosity and Ionic Conductivity

Figure 3a and b present an Arrhenius-like plot of viscosity for the $[P_{2225}][Tf_2N]$ and $[P_{222(2O1)}][Tf_2N]$ ILs and their $Li^+$ mixtures. The increase in temperature leads to a decrease in viscosity, as has been observed for others ILs that contain different cations[12] or anions.[38] The addition of $Li^+$ increases the viscosity because of the strong interaction between the metallic cation and the $Tf_2N^-$ anion, as already reported for ILs containing this

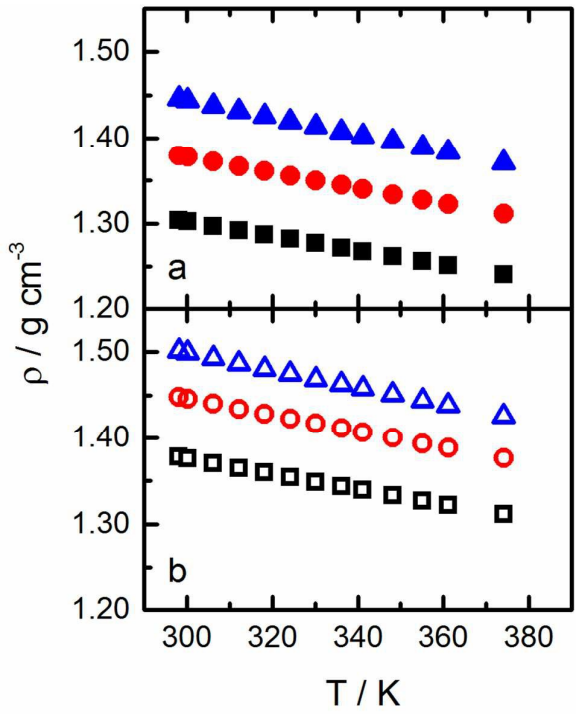


Figure 2. Density at different temperatures of $[P_{2225}][Tf_2N]$ (a) and $[P_{222(2O1)}][Tf_2N]$ (b) for the neat IL (■, □), 1.0 mol $L^{-1}$ (●, ○) and 2.0 mol $L^{-1}$ (▲, △) $Li^+$ mixtures.

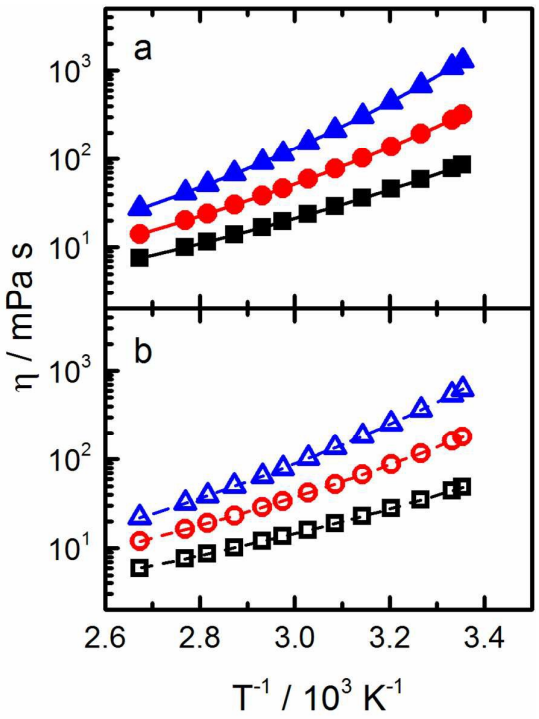


Figure 3. Arrhenius-like plot of viscosity of $[P_{2225}][Tf_2N]$ (a) and $[P_{222(2O1)}][Tf_2N]$ (b) for the neat IL (■, □), 1.0 mol $L^{-1}$ (●, ○) and 2.0 mol $L^{-1}$ (▲, △) $Li^+$ mixtures. Lines represent the best fits of the VTF equation.

Table 1. Experimental and calculated densities at 298 K.

| | $\rho_{exp.}$ (g $cm^{-3}$) | $\rho_{calc.}$ (g $cm^{-3}$) | error |
|---|---|---|---|
| $[P_{2225}][Tf_2N]$ | 1.3039 | 1.2843 | -1.5% |
| $[N_{2225}][Tf_2N]$ | 1.3105 | 1.2955 | -1.1% |
| $[Li]_{0.25}[P_{2225}]_{0.75}[Tf_2N]$ | 1.3797 | 1.3612 | -1.3% |
| $[Li]_{0.39}[P_{2225}]_{0.61}[Tf_2N]$ | 1.4460 | 1.4140 | -2.2% |
| $[P_{222(2O1)}][Tf_2N]$ | 1.3777 | 1.3539 | -1.7% |
| $[N_{222(2O1)}][Tf_2N]$ | 1.40 | 1.3696 | -2.2% |
| $[Li]_{0.25}[P_{222(2O1)}]_{0.75}[Tf_2N]$ | 1.4478 | 1.4254 | -1.5% |
| $[Li]_{0.39}[P_{222(2O1)}]_{0.61}[Tf_2N]$ | 1.5013 | 1.4765 | -1.7% |

Experimental densities for $[N_{2225}][Tf_2N]$ and $[N_{222(2O1)}][Tf_2N]$ were taken from [22] and [35], respectively.

anion.[14,39–41] At 298 K, neat $[P_{2225}][Tf_2N]$ has a viscosity 1.8 times larger than neat $[P_{222(2O1)}][Tf_2N]$.

The addition of $Li^+$ ions increases the viscosity by 3.8 (1.0 mol $L^{-1}$) and 15 (2.0 mol $L^{-1}$) times for $[P_{2225}][Tf_2N]$ relative to neat IL. In the case of $[P_{222(2O1)}][Tf_2N]$, the addition of $Li^+$ increases the viscosity by 3.7 (1.0 mol $L^{-1}$) and 13 (2.0 mol $L^{-1}$) times relative to neat IL. It is clear that the presence of an alkyl ether chain causes a diminution of the IL viscosity. Two explanations are given for this observation: first, the alkyl ether chain decreases the positive charge in the central atom, which decreases the electrostatic interaction between the ions;[21,42] second, the alkyl ether increases the chain flexibility, which increases ion mobility.[21,36,42] Although, the alkyl ether chain decreases the viscosity, it does not have any effect on the increase of viscosity by the addition of $Li^+$.

The data presented in Figure 3 can be fitted by the Vogel-Tammann-Fulcher (VTF) equation that follows:

$$\eta = \eta_0 \, exp\left(\frac{B}{T-T_0}\right) \quad (3)$$

where $\eta_0$, B and $T_0$ are adjustable parameters. The lines shown in Figure 3 represent the best VTF fit, and the parameters can be seen in Table S1. The relationship $B/T_0$ is inversely proportional to the liquid fragility. Thus, the fragility increases for a system relative to another when this parameter decreases. That is, the transport properties experience more change with temperature. When the $B/T_0$ parameter increases, the transport properties are less sensitive to changes in the temperature.[43,44] Usually, the strong/fragile classification is made near the glass transition temperature, but we will consider the liquid fragility only in the temperature range studied. However, possible modification to the $\eta(T)$ trend near the glass transition temperature must be considered.[45] For this reason, all $T_0$ parameters were fixed to 160 K for a better comparison, which is the value determined for neat $[P_{2225}][Tf_2N]$.[46] Neat $[P_{2225}][Tf_2N]$ is slightly more fragile than neat $[P_{222(2O1)}][Tf_2N]$. The two $Li^+$ concentrations increase the fragility in the same proportion for both ILs; indeed, the systems become more fragile as more $Li^+$ is added.

Figure 4a and b present an Arrhenius-like plot of ionic conductivity for $[P_{2225}][Tf_2N]$ and $[P_{222(2O1)}][Tf_2N]$ ILs and their $Li^+$ mixtures.

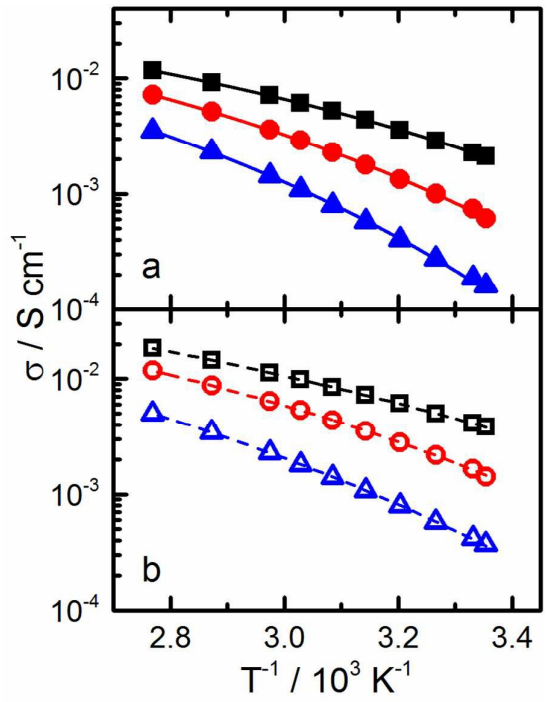


Figure 4. Arrhenius plot of ionic conductivity of $[P_{2225}][Tf_2N]$ (a) and $[P_{222(2O1)}][Tf_2N]$ (b) for the neat IL (■, □), 1.0 mol $L^{-1}$ (●, ○) and 2.0 mol $L^{-1}$ (▲, △) $Li^+$ mixtures. Lines represent the best fits of the VTF equation.

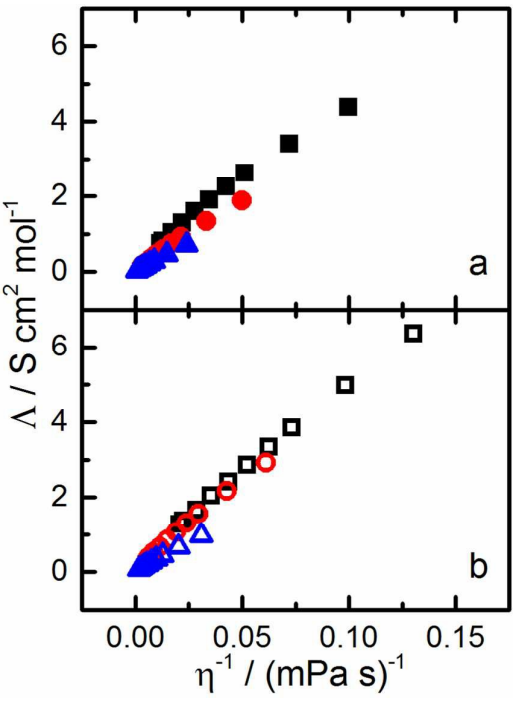


Figure 5. Relationship between the molar ionic conductivity and the fluidity (inverse of viscosity) of $[P_{2225}][Tf_2N]$ (a) and $[P_{222(2O1)}][Tf_2N]$ for the neat ILs (■, □), 1.0 mol $L^{-1}$ (●, ○) and 2.0 mol $L^{-1}$ (▲, △) $Li^+$ mixtures.

As in the case of viscosity, the ionic conductivity gives expected results. That is, it increases with the temperature for all systems examined and it decreases with the addition of $Li^+$. The ionic conductivity of neat $[P_{2225}][Tf_2N]$ is 1.8 times lower than neat $[P_{222(2O1)}][Tf_2N]$ (2.1 *vs.* 3.8 mS $cm^{-1}$, at 25 °C, respectively), indicating that the ionic conductivity is highly consistent with the viscosity. The addition of $Li^+$ causes a decrease of 3.4 and 13 times for $[P_{2225}][Tf_2N]$ (0.61 and 0.16 mS $cm^{-1}$, 25 °C, for 1.0 and 2.0 mol $L^{-1}$) and 2.7 and 10 times for $[P_{222(2O1)}][Tf_2N]$ (1.4 and 0.37 mS $cm^{-1}$, 25 °C, for 1.0 and 2.0 mol $L^{-1}$). The same logic used to rationalize the viscosity can be applied to understand the ionic conductivity; specifically, the alkyl ether chain permits a higher ionic mobility compared to the alkyl chain. The ionic conductivity also can be fitted by the VTF equation:

$$\sigma = \sigma_0 \, exp\left(\frac{-B}{T-T_0}\right) \quad (4)$$

where $\sigma_0$, B and $T_0$ are adjustable parameters and the lines represent the best VTF fit. The parameters can be seen in Table S2. The $B/T_0$ for all of the systems are in good agreement for those found in the viscosity analyses.

Figure 5a and b show the $\Lambda(\eta^{-1})$ plot for $[P_{2225}][Tf_2N]$ and $[P_{222(2O1)}][Tf_2N]$ ILs and their $Li^+$ mixtures. This representation is an effective way to analyze the relationship between the molar ionic conductivity and the liquid fluidity (i.e., the inverse of viscosity). All of the systems possess a linear relationship between molar ionic conductivity and fluidity. Thus, the increase in the ionic conductivity with temperature is directly related to the decrease in the viscosity, or the increase in fluidity.

The different slopes indicate different ionicities of the systems, which indicates how ideal an ionic liquid is.[47] The slopes of these lines are 42, 37 and 30 S $cm^2$ $mol^{-1}$ $mPa^{-1}$ $s^{-1}$ for $[P_{2225}][Tf_2N]$, $[Li]_{0.25}[P_{2225}]_{0.75}[Tf_2N]$ and $[Li]_{0.39}[P_{2225}]_{0.61}[Tf_2N]$, respectively, and 47, 46 and 31 S $cm^2$ $mol^{-1}$ $mPa^{-1}$ $s^{-1}$ for $[P_{222(2O1)}][Tf_2N]$, $[Li]_{0.25}[P_{222(2O1)}]_{0.75}[Tf_2N]$ and $[Li]_{0.39}[P_{222(2O1)}]_{0.61}[Tf_2N]$, respectively. Neat $[P_{222(2O1)}][Tf_2N]$ and its $Li^+$ counterpart have higher slopes than the analogues with the $P_{2225}^+$ cation. This finding is consistent with the notion that the alkyl ether chain improves ion mobility, which results in a higher molar ionic conductivity than those of the analogues with the $P_{2225}^+$ cation, assuming the same fluidity. The addition of $Li^+$ decreases the slope. This effect has been observed in other ILs containing the $Tf_2N^-$ anion but with a smaller diminution.[13] These results suggest that the presence of $Li^+$ does not have a decisive impact on the transport properties on the IL, as in the case of an IL with $Tf_2N^-$ and imidazolium.[13] Another important finding is the lower decrease of slope in the first $Li^+$ addition in the IL with $P_{222(2O1)}^+$ than in the IL with $P_{2225}^+$. This feature is well observed in the Walden plot (log $\Lambda$ vs log $\eta^{-1}$) in Figure S7. This may be related to the different ionicities of both systems. The alkyl ether chain guarantees a higher ionicity at lower $Li^+$ concentrations, resulting in a higher slope. However, when more $Li^+$ is added, the effect of the alkyl ether chain diminishes and the ionicity is similar to the IL containing an alkyl chain.

**Diffusion Coefficient**

The ions self-diffusivity were analyzed by PGSE-NMR, which allows one to calculate the self-diffusion coefficient, D, of each ion with $^{1}H$, $^{19}F$ and $^{7}Li$ nuclei to detect cations, anion and $Li^+$, respectively. Figure 6 presents an Arrhenius-like plot for D of the ions in both ILs and their $Li^+$ mixtures.

In the neat ILs, the $Tf_2N^-$ anion gives a slightly higher D than the cations in both ILs at most temperatures, which is contrary to the results of ILs containing imidazolium.[13] Comparing the $D_c$ between both ILs, we observe that the $P_{222(2O1)}^+$ cation has a higher D at all temperatures investigated (1.7 times, average) than the $P_{2225}^+$ cation. The $Tf_2N^-$ anion also has a higher D in the IL containing $P_{222(2O1)}^+$ (1.4 times, average).

As expected, the addition of $Li^+$ decreases the D of cations and anions since the systems become more viscous. The unexpected feature is the higher D for $Li^+$ than the other ions in the system at some temperatures. In ILs containing other cations, such imidazolium,[13] piperidinum[36] and pyrrolidinium,[48] the $Li^+$ possesses a lower D than the IL's ions, even though it has a smaller radius, since the agglomerates $Li^+$-anions result in stiffer systems and lower values of D.

The $Li^+$ ions are diffusing more freely in the ILs containing phosphonium cation. In the systems $[Li]_{0.25}[P_{222x}]_{0.75}[Tf_2N]$, the $P_{222(2O1)}^+$ cation has a D value that is, on average, 2.2 times higher than the $P_{2225}^+$ cation. The $Tf_2N^-$ anion has a D value that is 1.6 larger in the IL containing $P_{222(2O1)}^+$. In addition, $Li^+$ has a D value 1.4 larger in the IL containing $P_{222(2O1)}^+$.

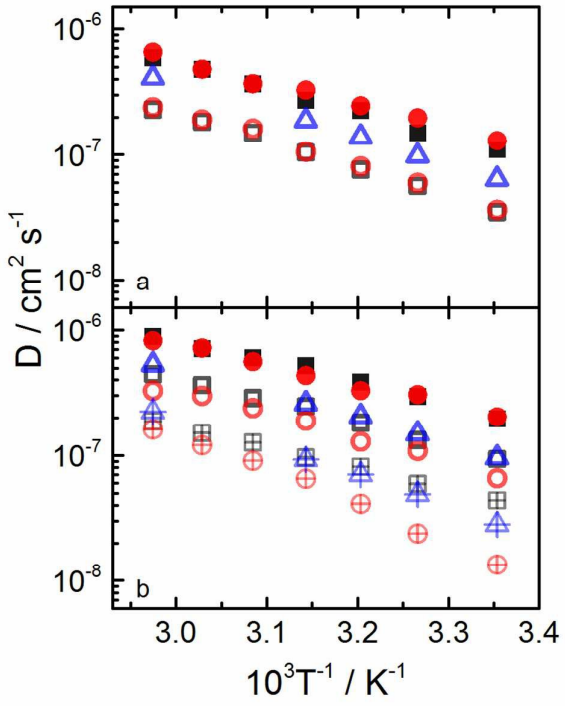


Figure 6. Arrhenius-like plot of the self-diffusion coefficient for the (a) $[P_{2225}][Tf_2N]$ and (b) $[P_{222(2O1)}][Tf_2N]$ calculated by PGSE-NMR. $P_{222x}^+$ (black square), $Tf_2N^-$ (red circles) and $Li^+$ (blue triangle). Full, open and crossed symbols represents the ions in neat IL, 1.0 and 2.0 mol $L^{-1}$ $Li^+$ mixtures, respectively.

These results indicate that the presence of the alkyl ether chain decreases the interaction among the ions, but it is not enough to completely break the aggregates $Li^+$-$Tf_2N^-$.

Considering the diffusion coefficients for the ions obtained by PGSE-NMR, one can calculate the ionic conductivity ($\sigma_{NMR}$) by the Nernst-Einstein equation and compare it with the experimental ionic conductivity ($\sigma_{exp}$). Figure 7 presents the relationship $\sigma_{exp}/\sigma_{NMR}$. If the ratio is 1.0, then all ions are available to carry charge. However, if the ratio is lower than 1.0, then the ions form neutral aggregates and their diffusion measured by PGSE-NMR is not related to ionic conductivity. The neat ILs containing phosphonium cation possess relatively high $\sigma_{exp}/\sigma_{NMR}$ ratios relative to ILs with other cations, indicating that fewer aggregations occur in the ILs with phosphonium than in the other ILs. The addition of $Li^+$ decreases the diffusion coefficient, *i.e.*, there are new aggregates that do not carry charge. Still, the $\sigma_{exp}/\sigma_{NMR}$ ratio for the $Li^+$ mixtures are considerably high for the mixtures that contain phosphonium cations relative to the other ILs.[13,36,49,50]

The transport number of $Li^+$ ($t_{Li+}$) was obtained by a technique proposed by Evans, Vincent and Bruce for polymeric electrolytes,[51] which consist of an EIS measurement at open circuit potential, a dc polarization followed by a second EIS measurement at the polarization potential, of a symmetrical cell of Li electrodes and the electrolyte in question. The following equation is used to calculate $t_{Li+}$:

$$t_{Li+} = \frac{i_{ss}(\Delta V - R_0 i_0)}{i_0(\Delta V - R_{ss} i_{ss})} \quad (5)$$

where $i_0$, $i_{ss}$ are the currents at initial and steady-state conditions, $R_0$ and $R_{ss}$ are the charge transfer resistances at initial and steady-state conditions, and $\Delta V$ is the dc polarization voltage, which is 10 mV in this work. Although the authors proposed the use of this procedure for polymeric electrolytes, many authors have used this procedure to calculate the $t_{Li+}$ in ILs,[11,50,52–54] see Figure S8 in Supplementary Information for more details. In addition, the diffusion coefficient of $Li^+$ was obtained by the reduction of $Li^+$ to Li using microelectrodes and using the equation $i_{ss}=4nFDC$, where $i_{ss}$ is the steady-state current, n is the number of electrons, F is the Faraday constant, D is the diffusion coefficient and C is the species concentration,[55,56] see Figure S9 in Supplementary Information for more details.

Table 2 shows the $Li^+$ diffusion coefficients and the $Li^+$ transport number calculated by PGSE-NMR ($D_{NMR}$ and $t_{NMR}$), the diffusion coefficient calculated using microelectrodes ($D_{Electrochem.}$) and the $Li^+$ transport number calculated by the electrochemical procedure described above ($t_{Electrochem.}$).

These three different techniques have different approaches to analyze $Li^+$ transport. PGSE-NMR considers both charged and neutral species, and the diffusion coefficient based on this technique is an average of the contributions from all the species containing the analyzed nuclei. In contrast, the diffusion calculation by Li electrodeposition and the Li transport number by the Evans, Vincent and Bruce method[51] consider only the $Li^+$ ion with charge. These two techniques do

not take in account the neutral aggregates between $Li^+$ and anions.

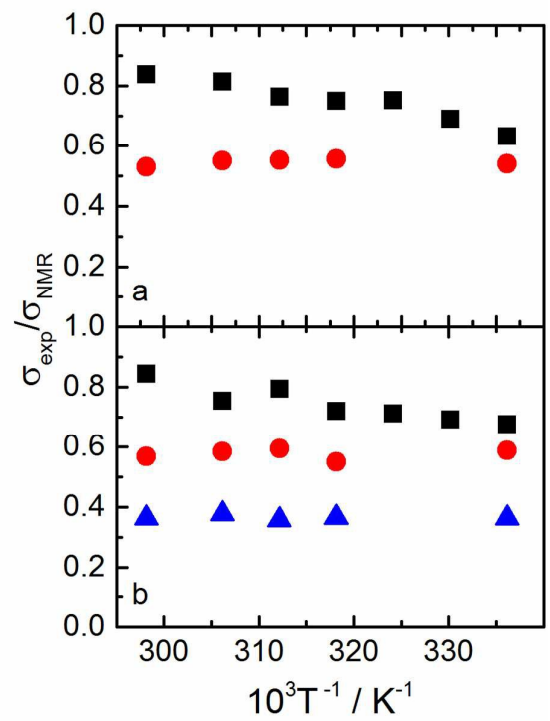


Figure 7. Relationship between the ionic conductivity calculated with the AC experiment and calculated by PGSE-NMR of $[P_{2225}][Tf_2N]$ (a) and $[P_{222(2O1)}][Tf_2N]$ (b) for neat IL (■) 1.0 mol $L^{-1}$ (●) and 2.0 mol $L^{-1}$ (▲) $Li^+$ mixtures.

Table 2. $Li^+$ diffusion coefficient and transport number obtained by PGSE-NMR and an electrochemical procedure at 25 °C.

| | $D_{NMR}$ ($10^{-7}$ $cm^2$ $s^{-1}$) | $t_{NMR}$ | $D_{Electrochem}$ ($10^{-7}$ $cm^2$ $s^{-1}$) | $t_{Electrochem}$ |
|---|---|---|---|---|
| $[Li]_{0.25}[P_{2225}]_{0.75}[Tf_2N]$ | 0.64 ± 0.01 | 0.24 ± 0.02 | 1.2 ± 0.3 | 0.44 ± 0.05 |
| $[Li]_{0.25}[P_{222(2O1)}]_{0.75}[Tf_2N]$ | 0.96 ± 0.01 | 0.17 ± 0.02 | 2.0 ± 0.4 | 0.54 ± 0.04 |

$t_{NMR}$ was calculated using $t_i = x_i D_i / \sum(xD)$

The $D_{Electrochem}$ values are twice as large as the $D_{NMR}$ values for both mixtures. This result indicates that the $Li^+$ ions which are not associated with or forming aggregates with the anion, *i.e.* those carrying charge, have higher diffusion coefficients. $D_{NMR}$ considers the neutral aggregates between the metallic cation and the anions, which are larger and more voluminous than the small charged $Li^+$, which carries charge. In addition, the $t_{Electrochem}$ are significantly higher than $t_{NMR}$, *e.g.*, 0.44 and 0.54 for the mixture containing the cations $P_{2225}^+$ and $P_{222(2O1)}^+$, respectively. These results confirm that the PGSE-NMR method underestimates the diffusion coefficient of charged species since it considers all the species and aggregates. Since the aggregates have a larger radius than $Li^+$, their low diffusion coefficients decrease the overall $Li^+$ diffusion coefficient and transport number. The $Li^+$ mixtures with ILs containing phosphonium cations possess high $Li^+$ transport numbers relative to similar systems,[11,50,52–54] suggesting that they may be promising electrolytes for lithium ion batteries.

### Raman Spectroscopy

The Raman spectra presented in Figure 8 show the region of the spectrum where it is possible to observe one intense band of the $Tf_2N^-$ anion. The band located at 740 $cm^{-1}$ is related to the expansion and contraction of the entire $Tf_2N^-$ anion[57] and it is very sensitive to the addition of $Li^+$.[13,57] When $Li^+$ salt is added to neat IL, this intense band is split into two bands, one at 742 $cm^{-1}$ and another at 747 $cm^{-1}$. The intensity of first band decreases and the second band increases as the concentration of $Li^+$ increases. The band at 742 $cm^{-1}$ is related to the free anions (weak aggregates) and the band at 747 $cm^{-1}$ is related to the anions in the $Li^+$ coordination sphere (strong aggregates).[13,15,57] The ratio between the integral area of the band at 747 $cm^{-1}$ and the integration of both bands is proportional to the amount of $Li^+$ added in similar systems.[13,15,57,58]

Taking this in account, one can compare the ratios with the two different cations studied in this work. The systems containing the $P_{2225}^+$ cation give a ratio of 0.34 and 0.53 for $[Li]_{0.25}[P_{2225}]_{0.75}[Tf_2N]$ and $[Li]_{0.39}[P_{2225}]_{0.61}[Tf_2N]$, respectively. In the case of the systems containing the $P_{222(2O1)}^+$ cation, the ratios are 0.36 and 0.54 for $[Li]_{0.25}[P_{222(2O1)}]_{0.75}[Tf_2N]$ and $[Li]_{0.39}[P_{222(2O1)}]_{0.61}[Tf_2N]$, respectively (see Figure S10). Thus, it appears that the alkyl ether chain does not have an impact on the formation of the aggregates. This point will be addressed in more detail in the next section.

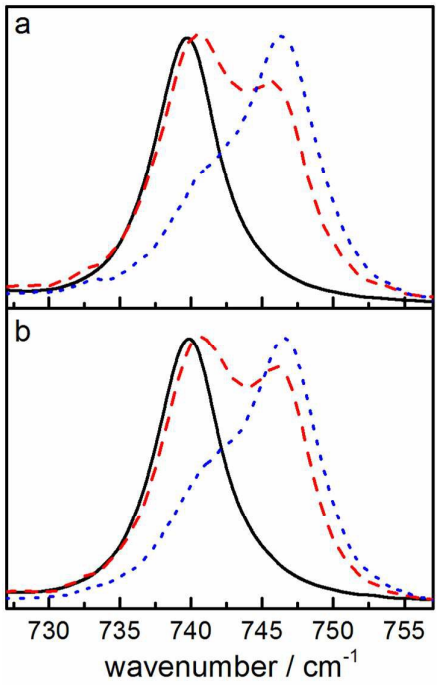


Figure 8. Raman spectra of (a) neat $[P_{2225}][Tf_2N]$ (black full line), $[Li]_{0.25}[P_{2225}]_{0.75}[Tf_2N]$ (red dashed line) and $[Li]_{0.39}[P_{2225}]_{0.61}[Tf_2N]$ (blue dotted line) and of (b) neat $[P_{222(2O1)}][Tf_2N]$ (black full line), $[Li]_{0.25}[P_{222(2O1)}]_{0.75}[Tf_2N]$ (red dashed line) and $[Li]_{0.39}[P_{222(2O1)}]_{0.61}[Tf_2N]$ (blue dotted line).

### Molecular Dynamics Simulations

Molecular dynamics (MDs) simulations were performed to obtain a better understanding of the short-range structure of the liquids. The radial distribution functions (rdf) were calculated between the P atom for the cation and the N atom for the anion, unless otherwise stated.

Figure 9a and b present the rdf for the neat ILs and the $Li^+$ mixtures for $P_{2225}^+$ and $P_{222(2O1)}^+$ cations, respectively.

The out-of-phase oscillation of the cross term with the cation-cation and anion-anion rdfs is observed because of the organization of the charge in the liquids.[59] At first view, both ILs (full lines) appear to possess similar short-range structures. The addition of $Li^+$ in ILs containing the $Tf_2N^-$ anion is known to disrupt anion-anion interactions. This change results in broad and undefined peaks with lower intensity than in neat IL because of the formation of relatively stiffer aggregates between the metallic cation and the anion.[13]

The different coordination numbers (CNs) found in the systems with different cations is noteworthy, as shown in Table 3. They were calculated with the rdf integration until the first minimum. The cation-cation and anion-anion CNs are *ca.* 1.4 times higher in the neat IL containing the $P_{222(2O1)}^+$ cation than in the IL containing $P_{2225}^+$. The cross term for the neat IL containing the $P_{222(2O1)}^+$ cation is 1.9 times higher than in the IL containing $P_{2225}^+$. The addition of $Li^+$ moves the coordination numbers to closer values in both systems, although the three CNs are still *ca.* 1.1 times higher for the $Li^+$ mixture containing the $P_{222(2O1)}^+$

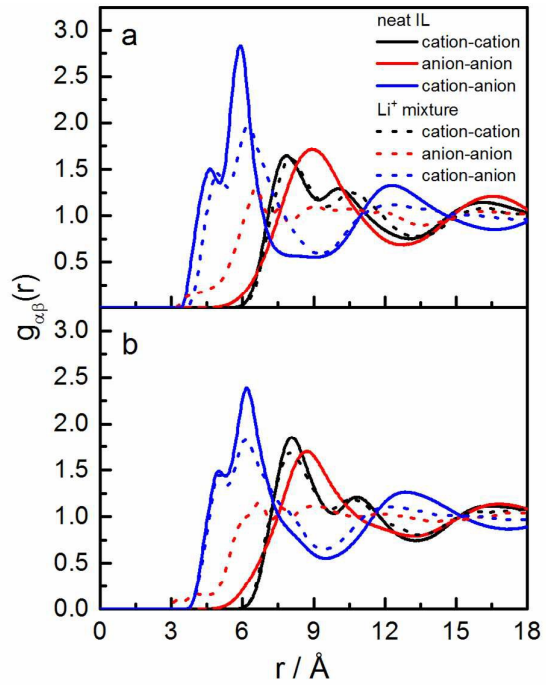


Figure 9. Radial distribution function between P-P (black lines), N-N (red lines) and P-N (blue lines) for (a) $[P_{2225}][Tf_2N]$ (full lines) and its $Li^+$ mixture (dashed lines) and (b) $[P_{222(2O1)}][Tf_2N]$ (full lines) and its $Li^+$ mixture (dashed lines). See legend for details. This figure is better observed in the color version.

Table 3. Coordination numbers for the systems simulated with MD, calculated by the integration of the g(r) until the first minimum (value indicated). Peaks with two important components are shown separately.

| | cation-cation | anion-anion | cross term |
|---|---|---|---|
| $[P_{2225}][Tf_2N]$ | 3.8 (9.2Å); 8.2 (13Å) | 11.5 (12.8Å) | 0.5 (5.0Å) 2.9 (7.9Å) |
| $[Li]_{0.25}[P_{2225}]_{0.75}[Tf_2N]$ | 4.8 (9.6Å) 9.8 (13.4Å) | 2.0 (7.1Å) 1.4 (8.0Å) | 0.9 (5.4Å) 6.1 (9.3Å) |
| $[P_{222(2O1)}][Tf_2N]$ | 6.7 (9.8Å) 10.1 (13.1Å) | 16.5 (13.1Å) | 0.72 (5.3Å) 5.9 (9.4Å) |
| $[Li]_{0.25}[P_{222(2O1)}]_{0.75}[Tf_2N]$ | 5.6 (9.7Å) 10.4 (13.5Å) | 2.2 (7.2Å) 1.5 (8.1Å) | 0.9 (5.4Å) 6.8 (9.4Å) |

cation. The systems containing the $P_{222(2O1)}^+$ cation are more densely packaged, resulting in an increase of the CNs.

Figure 10a and b show the rdfs of Li-anion for both mixtures. In particular, the rdfs of Li-N and Li-O are notable. The profiles are very similar to those observed in other IL containing the $Tf_2N^-$ anion.[13] The $Li^+$ is coordinated by *ca.* five O and three anions, suggesting that there are two bidentate anions and one monodentate ligand.[13] Both mixtures show very similar results. Thus, the different cations do not affect the way in which $Li^+$ is coordinated to $Tf_2N^-$ when the concentration is the same.

The combined distribution functions (cdfs) shown in Figure 11 present the rdf between one atom of the alkyl side chain (C6 for the $P_{2225}^+$ and O1 for the $P_{222(2O1)}^+$, see Figure S11 in SI) and the $Li^+$, combined with the angular distribution function (adf) between two vectors: the vector between P and C6 or O1 and the vector between $Li^+$ and C6 or O1 (see cartoon in Figure 11).

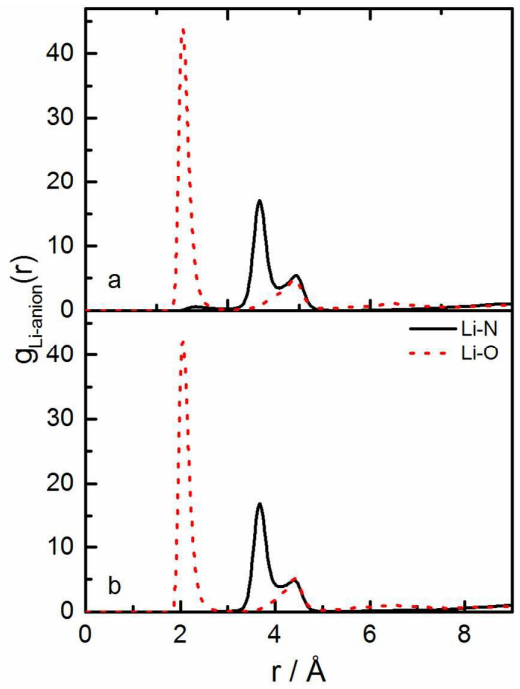


Figure 10. Radial distribution function between $Li^+$ and the $Tf_2N^-$ anion (N and O) for the $Li^+$ mixtures of (a) $[P_{2225}][Tf_{2N}]$ and (b) $[P_{222(2O1)}][Tf_2N]$. Li-N in full black lines and Li-O in dashed red lines.

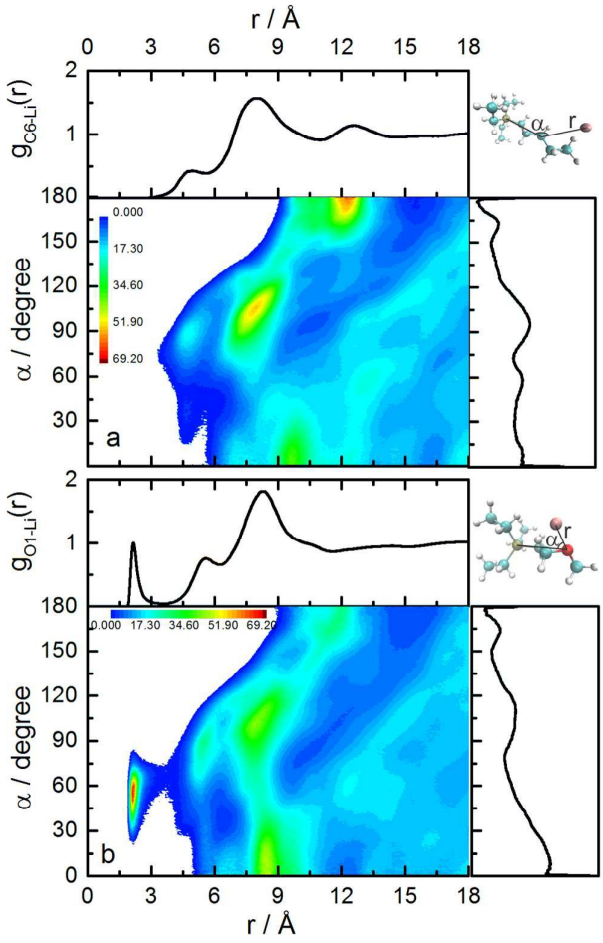


Figure 11. Combined distribution function of radial (rdf) and angular (adf) distribution functions for the $Li^+$ mixtures of $[P_{2225}][Tf_2N]$ (a) and $[P_{222(2O1)}][Tf_2N]$ (b). Rdf between C6 and $Li^+$ ($[P_{2225}][Tf_2N]$), O1 and $Li^+$ ($[P_{222(2O1)}][Tf_2N]$). Adf between the vectors P-C6-$Li^+$ ($[P_{2225}][Tf_2N]$) and P-O1-$Li^+$ ($[P_{222(2O1)}][Tf_2N]$).

In general, it is possible to evaluate the distance between $Li^+$ and the atom from the alkyl chain and the angle distribution between both vectors mentioned before.

Figure 11a presents the cdf for the $Li^+$ mixture containing the $P_{2225}^+$ cation. The first main peak for C6-Li is located at 8.0 Å and is related to 8.6 $Li^+$ around the C6, taking in account the first minor peak at 4.8 Å. The majority of these $Li^+$ have an angle between 80 and 120°, with a higher proportion having an angle of 105° relative to the vectors P-C6 and C6-Li. Additionally, Figure 11b presents the cdf for the $Li^+$ mixture containing the $P_{222(2O1)}^+$ cation. As in the previous case, two peaks are observed at approximately 5.5 and 8.2 Å and are related to 11 $Li^+$. The angles formed between the vectors P-O1 and O1-Li for the main peak at 8.2 Å are identical and the higher intensity occurs at an angle of 103°. The main difference between the cdfs is the presence of a sharp peak in the rdf for Li-O1 at 2.1 Å. In this case, the angle of the vectors related to this peak is *ca.* 60°. Although this peak is associated with a low CN (only 0.1 $Li^+$ around O1), it is important to note that some aggregates have a metallic cation closer to the

phosphonium cation when an alkyl ether side chain is present. This phenomenon is better observed in the spatial distribution functions shown in Figure 12.

Figure 12 shows the spatial distribution of the anion $Tf2N^-$ (light pink) and $Li^+$ (blue) around the cations $P_{2225}^+$ (Figure 12a) and $P_{222(2O1)}^+$ (Figure 12b). It is clear that the alkyl ether chain causes a modification to the short-range structure around the cation.

Although a low probability, it is possible that the metallic cation moves closer to the phosphonium cation than the $Tf_2N^-$ anion.

The results from Figure 11 and Figure 12 are in agreement with the results from Figure 5. The higher slope for $\Lambda$ *vs* $\eta^{-1}$ observed in Figure 5 for the $Li^+$ mixture containing $P_{222(2O1)}^+$ than for the $Li^+$ mixture containing $P_{2225}^+$ must be related to the slightly higher interaction between metallic cations and organic cations for the IL with the alkyl ether chain, as observed in Figure 11 and Figure 12.

## Conclusions

In summary, the ILs containing phosphonium cations possess interesting properties that can be viewed as potential electrolytes for Li-ion batteries. The ILs have a wide electrochemical window and ionic conductivity. Moreover, even with the addition of $Li^+$, the mixtures still possess relatively high ionicity compared with ILs containing other cations. The $Li^+$ mixture of the IL containing the cation with an alky ether chain possesses a higher ionicity than its analogue with an alkyl chain, as demonstrated by PGSE-NMR, the $Li^+$ diffusion coefficient and transport number calculations. The results from Raman spectroscopy suggest that the aggregates formed between $Li^+$ and the anion are similar to the aggregates formed in ILs containing others cations. Even the ILs containing an alky ether chain and an alky chain appear to possess similar aggregates. The MD simulations showed that although the number of neighbours around $Li^+$ is similar in both ILs, $Li^+$ can be found near the alkyl ether chain with a higher probability than it can be found near the alkyl chain. The presence of the alkyl ether chain changes the way that $Li^+$ interacts with the IL cation. In order to have a better description of the systems regarding the application as electrolytes for Li-ion batteries, further analyses must be done. One must considerer the properties of the Solid Electrolyte Interphase formed from the reaction between the mixtures and the electrodes, as the graphitic anode and the metals oxide cathode.

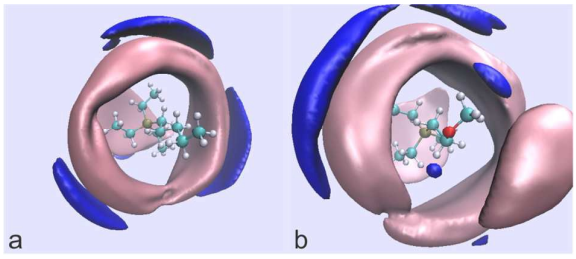


Figure 12. Spatial distribution function of the centre of mass of the $Tf_2N^-$ anion (light pink) and $Li^+$ cation (blue) around the $P_{2225}^+$ (a) and $P_{222(2O1)}^+$ (b) cations.

## Acknowledgments

The authors acknowledge FAPESP (09/53199-3) for financial support. NSR and VLM thank FAPESP (10/08646-9, 14/01987-6 and 13/22748-7, respectively) for fellowship support.

## References

1. D. R. MacFarlane, J. M. Pringle, K. M. Johansson, S. Forsyth, and M. Forsyth, *Chem. Commun.*, 2006, 1905–17.
2. M. Armand, F. Endres, D. R. MacFarlane, H. Ohno, and B. Scrosati, *Nat. Mater.*, 2009, **8**, 621–629.
3. M. Kosmulski, J. Gustafsson, and J. B. Rosenholm, *Thermochim. Acta*, 2004, **412**, 47–53.
4. L. Zhao, J. Yamaki, and M. Egashira, *J. Power Sources*, 2007, **174**, 352–358.
5. B. Garcia, S. Lavallée, G. Perron, C. Michot, and M. Armand, *Electrochim. Acta*, 2004, **49**, 4583–4588.
6. P. Simon and Y. Gogotsi, *Nat. Mater.*, 2008, **7**, 845–54.
7. M. Balaish, A. Kraytsberg, and Y. Ein-Eli, *Phys. Chem. Chem. Phys.*, 2014, **16**, 2801–2822.
8. H. Sakaebe, H. Matsumoto, and K. Tatsumi, *Electrochim. Acta*, 2007, **53**, 1048–1054.
9. B. Scrosati and J. Garche, *J. Power Sources*, 2010, **195**, 2419–2430.
10. T. Evans, J. Olson, V. Bhat, and S.-H. Lee, *J. Power Sources*, 2014, **269**, 616–620.
11. A. Fernicola, F. Croce, B. Scrosati, T. Watanabe, and H. Ohno, *J. Power Sources*, 2007, **174**, 342–348.
12. F. F. C. Bazito, Y. Kawano, and R. M. Torresi, *Electrochim. Acta*, 2007, **52**, 6427–6437.
13. M. J. Monteiro, F. F. C. Bazito, L. J. A. Siqueira, M. C. C. Ribeiro, and R. M. Torresi, *J. Phys. Chem. B*, 2008, **112**, 2102–2109.
14. Y. Umebayashi, H. Harnano, S. Seki, B. Minofar, K. Fujii, K. Hayamizu, S. Tsuzuki, Y. Kameda, S. Kohara, and M. Watanabe, *J. Phys. Chem. B*, 2011, **115**, 12179–12191.
15. K. Fujii, T. Fujimori, T. Takamuku, R. Kanzaki, Y. Umebayashi, and S.-I. Ishiguro, *J. Phys. Chem. B*, 2006, **110**, 8179–83.
16. K. J. Fraser and D. R. MacFarlane, *Aust. J. Chem.*, 2009, **62**, 309.
17. C. J. Bradaric, A. Downard, C. Kennedy, A. J. Robertson, and Y. Zhou, *Green Chem.*, 2003, **5**, 143–152.
18. K. Tsunashima, E. Niwa, S. Kodama, M. Sugiya, and Y. Ono, *J. Phys. Chem. B*, 2009, **113**, 15870–15874.
19. F. Atefi, M. T. Garcia, R. D. Singer, and P. J. Scammells, *Green Chem.*, 2009, 11, 1595–1604.
20. K. Tsunashima and M. Sugiya, *Electrochemistry*, 2007, **75**, 734.
21. K. Tsunashima and M. Sugiya, *Electrochem. commun.*, 2007, **9**, 2353–2358.
22. S. Seki, K. Hayamizu, S. Tsuzuki, K. Fujii, Y. Umebayashi, T. Mitsugi, T. Kobayashi, Y. Ohno, Y. Kobayashi, Y. Mita, H. Miyashiro, and S. Ishiguro, *Phys. Chem. Chem. Phys.*, 2009, **11**, 3509–14.
23. G. M. A. Girard, M. Hilder, H. Zhu, D. Nucciarone, K. Whitbread, S. Zavorine, M. Moser, M. Forsyth, D. R. MacFarlane, and P. C. Howlett, *Phys. Chem. Chem. Phys.*, 2015, **17**, 8706–8713.
24. K. Tsunashima, F. Yonekawa, and M. Sugiya, *Chem. Lett.*, 2008, 37, 314–315.
25. T. R. L. C. Paixão and M. Bertotti, *Electrochem. commun.*, 2008, **10**, 1180–1183.
26. J. Evans, C. A. Vincent, and P. G. Bruce, *Polymer (Guildf).*, 1987, **28**, 2324–2328.
27. T. M. Benedetti and R. M. Torresi, *Langmuir*, 2013, **29**, 15589–95.

28. W. Smith and T. R. Forester, *J. Mol. Graph.*, 1996, **14**, 136–141.
29. X. Liu, Y. Zhao, X. Zhang, G. Zhou, and S. Zhang, *J. Phys. Chem. B*, 2012, **116**, 4934–42.
30. J. N. Canongia Lopes and A. A. H. Pádua, *J. Phys. Chem. B*, 2004, **108**, 16893–16898.
31. J. Aaqvist, *J. Phys. Chem.*, 1990, **94**, 8021–8024.
32. L. Martínez, R. Andrade, E. G. Birgin, and J. M. Martínez, *J. Comput. Chem.*, 2009, **30**, 2157–2164.
33. W. C. Swope, H. C. Andersen, P. H. Berens, and K. R. Wilson, *J. Chem. Phys.*, 1982, **76**, 637–649.
34. M. Brehm and B. Kirchner, *J. Chem. Inf. Model.*, 2011, **51**, 2007–2023.
35. Z.-B. Zhou, H. Matsumoto, and K. Tatsumi, *Chemistry*, 2005, **11**, 752–66.
36. M. J. Monteiro, F. F. Camilo, M. C. C. Ribeiro, and R. M. Torresi, *J. Phys. Chem. B*, 2010, **114**, 12488–12494.
37. C. Ye and J. M. Shreeve, *J. Phys. Chem. A*, 2007, **111**, 1456–1461.
38. N. Sanchez-Ramirez, V. L. Martins, R. A. Ando, F. F. Camilo, S. M. Urahata, M. C. C. Ribeiro, and R. M. Torresi, *J. Phys. Chem. B*, 2014, **118**, 8772–8781.
39. K. Fujii, H. Hamano, H. Doi, X. Song, S. Tsuzuki, K. Hayamizu, S. Seki, Y. Kameda, K. Dokko, M. Watanabe, and Y. Umebayashi, *J. Phys. Chem. C*, 2013, **117**, 19314–19324.
40. Y. Umebayashi, T. Mitsugi, S. Fukuda, T. Fujimori, K. Fujii, R. Kanzaki, M. Takeuchi, and S.-I. Ishiguro, *J. Phys. Chem. B*, 2007, **111**, 13028–13032.
41. B. G. Nicolau, A. Sturlaugson, K. Fruchey, M. C. C. Ribeiro, and M. D. Fayer, *J. Phys. Chem. B*, 2010, **114**, 8350–8356.
42. T. Sato, G. Masuda, and K. Takagi, *Electrochim. Acta*, 2004, **49**, 3603–3611.
43. C. A. Angell, *Chem. Rev.*, 2002, **102**, 2627–2650.
44. W. Xu, E. I. Cooper, and C. A. Angell, *J. Phys. Chem. B*, 2003, **107**, 6170–6178.
45. M. C. C. Ribeiro, *J. Chem. Phys.*, 2010, **133**, 024503–1–024503–6.
46. V. Lesch, S. Jeremias, A. Moretti, S. Passerini, A. Heuer, and O. Borodin, *J. Phys. Chem. B*, 2014, **118**, 7367–7375.
47. K. Ueno, Z. Zhao, M. Watanabe, and C. A. Angell, *J. Phys. Chem. B*, 2012, **116**, 63–70.
48. F. Castiglione, E. Ragg, A. Mele, G. B. Appetecchi, M. Montanino, and S. Passerini, *J. Phys. Chem. Lett.*, 2011, **2**, 153–157.
49. K. Hayamizu, Y. Aihara, H. Nakagawa, T. Nukuda, and W. S. Price, *J. Phys. Chem. B*, 2004, **108**, 19527–19532.
50. H. Yoon, P. C. Howlett, A. S. Best, M. Forsyth, and D. R. MacFarlane, *J. Electrochem. Soc.*, 2013, **160**, A1629–A1637.
51. P. Bruce, J. Evans, and C. Vincent, *Solid State Ionics*, 1988, **28-30**, 918–922.
52. S. Seki, Y. Ohno, H. Miyashiro, Y. Kobayashi, A. Usami, Y. Mita, N. Terada, K. Hayamizu, S. Tsuzuki, and M. Watanabe, *J. Electrochem. Soc.*, 2008, **155**, A421–A427.
53. S. Ferrari, E. Quartarone, P. Mustarelli, A. Magistris, S. Protti, S. Lazzaroni, M. Fagnoni, and A. Albini, *J. Power Sources*, 2009, **194**, 45–50.
54. H.-B. Han, K. Liu, S.-W. Feng, S.-S. Zhou, W.-F. Feng, J. Nie, H. Li, X.-J. Huang, H. Matsumoto, M. Armand, and Z.-B. Zhou, *Electrochim. Acta*, 2010, **55**, 7134–7144.
55. B. C. M. Martindale, S. E. Ward Jones, and R. G. Compton, *Phys. Chem. Chem. Phys.*, 2010, **12**, 1827–33.
56. L. Lodovico, V. L. Martins, T. M. Benedetti, and R. M. Torresi, *J. Braz. Chem. Soc.*, 2014, **25**, 460–468.
57. J.-C. Lassegues, J. Grondin, and D. Talaga, *Phys. Chem. Chem. Phys.*, 2006, **8**, 5629–5632.
58. V. L. Martins, B. G. Nicolau, S. M. Urahata, M. C. C. Ribeiro, and R. M. Torresi, *J. Phys. Chem. B*, 2013, **117**, 8782–8792.
59. L. J. A. Siqueira and M. C. C. Ribeiro, *J. Chem. Phys.*, 2011, **135**, 204506–1 – 204506–7.